Pinning field representation using play hysterons for stress-dependent domain-structure model

Tetsuji Matsuo[1,*], Yasuhito Takahashi[2], and Koji Fujiwara[2]

[1]Graduate School of Engineering, Kyoto University, Kyoto 615-8510, Japan
[2]Doshisha University, 1-3, Tatara Miyakodani, Kyotanabe, Kyoto 610-0321, Japan
*Corresponding author: matsuo.tetsuji.5u@kyoto-u.ac.jp

Abstract: To predict the stress-dependent magnetization properties of silicon steel using a multiscale magnetization model called assembled domain structure model, pinning field models are developed using the play model. The hysteretic property of pinning field is identified from measured BH loops under stress-free condition. From the unidirectional hysteretic property, the distribution of the play hysterons is determined via an identification method that uses scalar and vector play models under the assumption of 2D or 3D distribution of crystal orientations. The loss properties of non-oriented silicon steel under compressive and tensile stresses are predicted successfully using an energy minimization process without parameter fitting to the stress-dependent measurement results.

Keywords: Hysteresis loss, magnetization analysis, mechanical stress, play model.

1. INTRODUCTION

The increased losses that occur in iron core materials as a result of mechanical stress can reduce motor efficiency through the shrink fitting process. To study the effects of stress, the stress-dependent loss properties have been measured widely in recent years [1]-[4]. These measured stress-dependent properties are then often phenomenologically modeled for use in magnetic field analysis of electric machines. However, performing these measurements under all the vector/tensor combinations of the magnetization and stress directions is impossible in practice. Therefore, a physical magnetization model [5]-[7] is required that can predict the stress-dependent properties from basic material constants such as the material's anisotropy constant and magnetostriction constants.

The assembled domain structure model (ADSM) [7] is an energy-based physical magnetization model that has been used successfully to predict the increased losses due to mechanical stress [8].

The ADSM yields the hysteretic properties of materials using the pinning field accompanied by the domain wall motion. The pinning field distribution is given using a Gaussian function that was determined in a trial-and-error manner. The behavior of the pinning field and its dependence on the distribution is reconstructed using the stop model to impose the pinning field on every cell in the ADSM. In [9], a direct identification method was developed to construct a stop model from the measured hysteretic properties under stress-free conditions. The stop model [10] is a convenient model for representation of the relationship between the input magnetization M and the output magnetic field H. The play model [10], [11] is also an accurate hysteresis model that can represent the relationship between M and H. This study examines pinning field modeling when using the play model. The paper presents a method for direct identification of the pinning field distribution using scalar and vector play models.

2. MULTI-DOMAIN PARTICLE MODEL

2.1. ADSM

The ADSM [7] is a multiscale model in which macroscopic magnetization is constructed by assembling mesoscopic cells on the crystal grain scale; these cells are called simplified domain structure models (SDSMs [12]). The magnetization state in each cell is determined to give the local minimum of the total magnetic energy, which comprises the Zeeman energy, the crystalline anisotropy energy, the magnetostatic energy, and the magnetoelastic energy. See the Appendix A for a brief explanation of the ADSM.

The pinning field h_{pn} accompanied by the domain wall motion of domain i can be represented by the stop model as follows [8]:

$$h_{\mathrm{pn}} = S(2r_i - 1) \tag{1}$$

where S is a hysteretic function that is described by the scalar stop model and r_i is the volume ratio of domain i. In a previous study, the distribution of the pinning field was first assumed to take the form of a Gaussian function. Then, based on the resulting hysteretic properties, the stop model was identified to constitute S in (1). From a physical viewpoint, the distribution can be determined using the density of the impurities contained in the material and the geometry of the crystal grains; however, these properties are difficult to determine. Reference [9] used a hysteretic property that was measured under stress-free conditions to identify the stop model directly.

2.2. Pinning Field Represented by Play Model

Use of the stop model is a natural choice to represent the hysteretic function from the input of the normalized magnetization m to the output of the normalized magnetic field h. However, the play model can also represent the hysteretic function from m to h. In addition, the play model can describe the hysteretic function from the input magnetic flux density to the output magnetic field in silicon steel more accurately than the stop model [10].

This paper examines the play model for use in pinning field modeling. The stop model in (1) is replaced by the play model as follows.

If a single crystal of a magnetic material has a two-domain state with a 180° domain wall, the volume ratios of the two domains r_i and $1-r_i$ give the normalized magnetization $m = 2r_i-1$. Therefore, the applied field along the magnetization direction yields the pinning field that can be represented by the scalar play model having an input m and an output h_{pn} as

$$h_{\mathrm{pn}} = P(2r_i-1)\ . \tag{2}$$

Therein P is a hysteretic function described by the scalar play model P_1 [11]:

$$P_1(m) = F_1(m) + \int_{+0}^{m_S} f_1(\zeta, p_\zeta(m))\ \mathrm{d}\zeta \tag{3}$$

where $m_S = 1$ is the normalized saturation magnetization, f_1 is a shape function, and $F_1(m)$ is a reversible component of $P_1(m)$. The play hysteron p_ζ, which has a width of ζ, is defined as

$$p_\zeta(m) = \max(\min(p_\zeta^0, m+\zeta), m-\zeta) \tag{4}$$

where p_ζ^0 represents the values of p_ζ at the previous time point.

The pinning field given in (2) is generated by every domain i (i = 1, …, 6), even when $r_i = 0$ and when domain i makes no contribution to the cell magnetization. This paper modifies the pinning model accordingly as

$$h_{\mathrm{pn}} = r_i\, P(2r_i-1) \tag{5}$$

which means that the pinning field in a cell is weighted by the volume ratios of the domains. This is called a weighted pinning field model, whereas the pinning model given by (2) is called an unweighted model.

The polycrystalline magnetic material with random crystal orientations is represented using the ADSM, which consists of cells with uniformly distributed crystal orientations. If the crystal orientation is uniformly distributed two-dimensionally, it is then assumed that the total pinning field is represented approximately by a 2D isotropic vector play model constructed via the superposition of scalar play models [11]

$$\boldsymbol{H} = \boldsymbol{P}(\boldsymbol{m}) = \int_{-\pi/2}^{\pi/2} \boldsymbol{e}_\varphi P_2(\boldsymbol{e}_\varphi \cdot \boldsymbol{m})\, \mathrm{d}\varphi \tag{6}$$

where $\boldsymbol{e}_\varphi$ is the unit vector along the φ-direction and $P_2(m)$ is a scalar play model that is given using the same form as (3). For a three-dimensional distribution, a 3D isotropic vector play model [13] is used as follows:

$$\boldsymbol{H} = \boldsymbol{P}(\boldsymbol{m}) = \int_0^{2\pi}\int_0^{\pi/2} \boldsymbol{e}_{\theta,\varphi} P_3(\boldsymbol{e}_{\theta,\varphi} \cdot \boldsymbol{m}) \sin\theta\, \mathrm{d}\theta\, \mathrm{d}\varphi \tag{7}$$

where $P_3(m)$ is a scalar play model and $\boldsymbol{e}_{\theta,\varphi}$ is the unit vector along the (θ, φ)-direction.

The scalar paly models P_2 and P_3 are then identified using a measured unidirectional property. For identification, the following function T_k (where k =1, 2, 3) is defined.

$$T_k(\zeta, p) = \begin{cases} F_k(p) + \int_{+0}^{\zeta} f_k(\xi, p)\ \mathrm{d}\xi & (0 < \zeta) \\ F_k(p) & (\zeta = 0) \end{cases}. \tag{8}$$

In (8), F_k and f_k denote the reversible component and the shape function of P_k, respectively. In order for the vector play models (6) and (7) to have unidirectional properties that are the same as the scalar hysteretic property given by the scalar play model P_1, T_2 and T_3 should satisfy [11][13]

$$T_1(\zeta, p) = \int_{-\pi/2}^{\pi/2} T_2(\zeta\cos\varphi, p\cos\varphi)\cos\varphi \,\mathrm{d}\varphi\,, \tag{9}$$

$$T_1(\zeta, p) = 2\pi\int_{0}^{\pi/2} T_3(\zeta\cos\theta, p\cos\theta)\cos\theta\sin\theta \,\mathrm{d}\theta\,. \tag{10}$$

The integral equations (9) (10) for T_2 and T_3 are solved as:

$$T_2(\zeta, p) = \frac{1}{\pi}\int_{0}^{\pi/2} T_{12}(\zeta\cos\varphi, p\cos\varphi)\mathrm{d}\varphi \tag{11}$$

$$T_3(\zeta, p) = \frac{1}{2\pi}[2T_1(\zeta, p) + \zeta\frac{\partial T_1(\zeta, p)}{\partial\zeta} + p\frac{\partial T_1(\zeta, p)}{\partial p}] \tag{12}$$

where

$$T_{12}(\zeta, p) = T_1(\zeta, p) + \zeta\frac{\partial T_1(\zeta, p)}{\partial\zeta} + p\frac{\partial T_1(\zeta, p)}{\partial p}\,. \tag{13}$$

The functions f_k and F_k (k = 2, 3) are then obtained from T_k as:

$$F_k(p) = T_k(0, p)\,,\quad f_k(\zeta, p) = \frac{\partial T_k(\zeta, p)}{\partial\zeta}\ (0 < \zeta)\,. \tag{14}$$

First, the anhysteretic property is removed from the measured hysteretic properties to extract the pinning field component, from which the scalar play model P_1 can then be identified. After obtaining the shape functions f_1 and F_1 of P_1, T_1 is found from (8) and is used to determine the shape functions f_k and F_k from T_k (k = 2, 3) using (11)–(13) for the 2D and 3D models.

3. Numerical Results

The stress-dependent magnetic properties of a nonoriented steel sheet (JIS: 50A470) were measured using a stress-loading single-sheet tester [14], where a strip sample was attached with a glass epoxy plate to prevent buckling; one end of the sample was fixed and the other end was pushed/pulled mechanically. From the catalogue data for the mass density, the silicon weight ratio in this steel is estimated to be approximately 3%, which gives an anisotropy constant for the cubic anisotropy of $K = 4.2\times10^4$ J/m^3, while the magnetostriction constants are $\lambda_{100} = 2.4\times10^{-5}$, $\lambda_{111} = -9.5\times10^{-6}$ and $\mu_0 M_S = 2.07$ T [15]-[17]. From the hysteretic properties that were measured under stress-free conditions, the scalar play models P_k (k = 1, 2, 3) can be identified. The pinning fields that are represented by these play models are shown in Fig. 1. However, the cell assembly is not equivalent to the superpositions in (6) or (7). Therefore, depending on the pinning model, each shape function pair (f_k, F_k) is multiplied by a constant to adjust the pinning field strength under stress-free conditions.

The magnetization process is simulated using 64 cells with uniformly distributed crystal orientations.

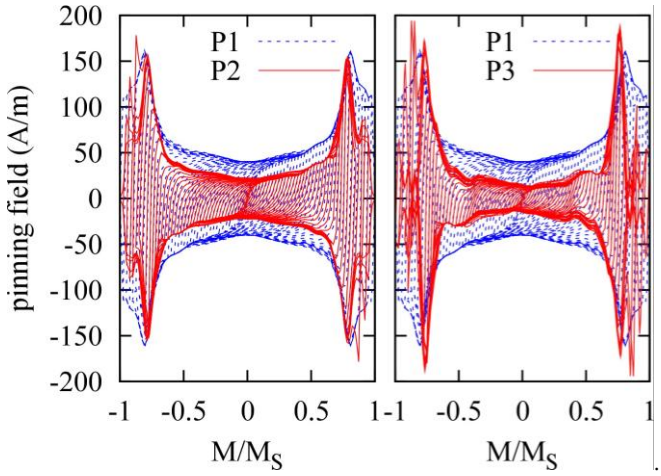

Fig. 1. Pinning fields represented by play models P_1, P_2, and P_3.

The hysteresis loss per cycle with and without the compressive stress is plotted in Fig. 2, where the pinning field h_{pn} in the ADSM is determined by the scalar play model $P = P_1$, P_2 or P_3. The increased loss caused by the compressive stress is predicted accurately by both the weighted model (2) and unweighted model (5). The simulated BH loops are drawn in Fig.

3. The loops under compressive stress of 40 MPa are predicted roughly without parameter fitting to the measured data under the mechanical stress. There are no major differences between the unweighted and weighted pinning field models. Despite the pinning field distribution differences shown in Fig. 1, the three scalar play models yield approximately the same properties.

The stress dependence of the hysteresis loss per cycle with an amplitude of 1.48 T is reconstructed in Fig. 4, in which a large increase in loss under compressive stress and a small decrease in loss under tensile stress are predicted. The weighted pinning field model provides slightly more accurate loss prediction than the unweighted model.

A comparison with the stop model is discussed in Appendix B.

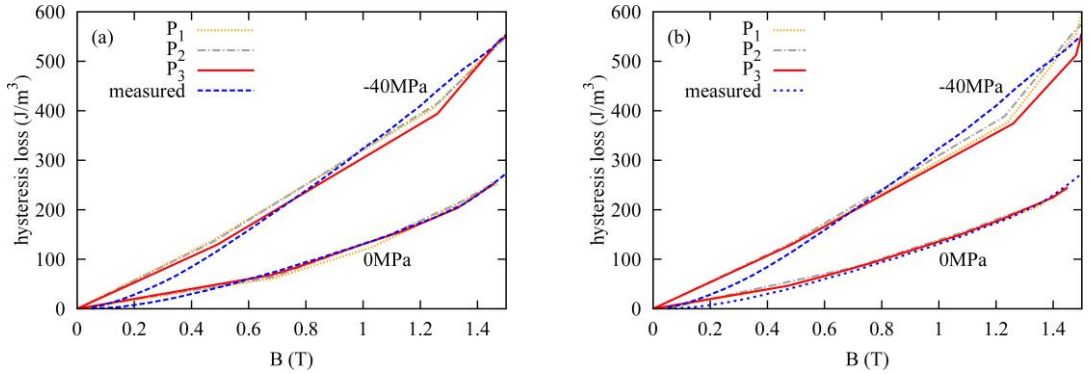

Fig. 2. Hysteresis losses per cycle with and without compressive stress of 40 MPa using the (a) unweighted and (b) weighted pinning field models, where the scaler play model P is given by P_1, P_2 or P_3.

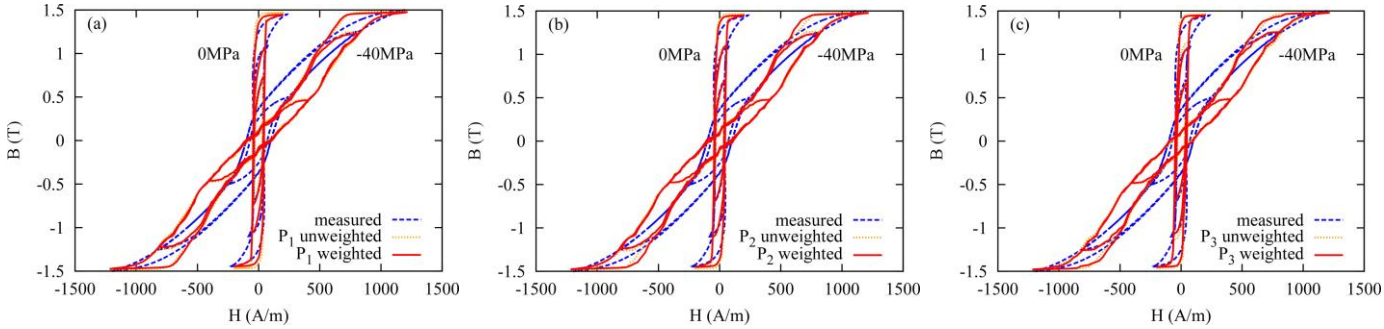

Fig. 3. BH loops simulated using the scalar play model P for pinning field distribution with unweighted model (2) and weighted model (5): (a) $P = P_1$, (b) $P = P_2$, and (c) $P = P_3$.

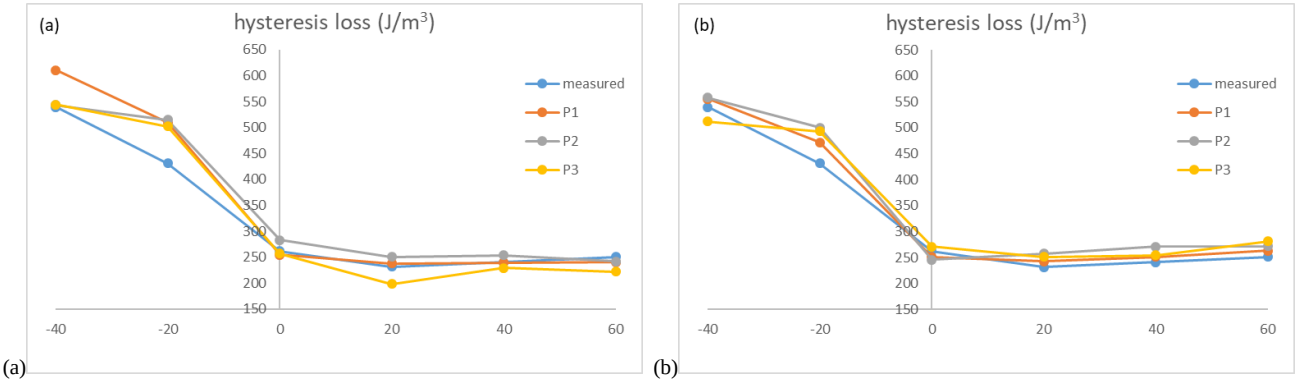

Fig. 4. Stress dependence of the hysteresis loss when using (a) unweighted and (b) weighted pinning field models with $P = P_1$, P_2, and P_3.

4. Conclusions

The pinning field is modeled for the ADSM using the scalar play model, where the play model is directly identified from BH loops measured unidirectionally under stress-free conditions using the theory of the vector play model. The proposed model predicts the stress-dependent magnetization properties successfully without any parameter fitting to previously measured data under mechanical stress, where not only a large increase in iron-loss under compressive stress but also a small decrease in loss under tensile stress are estimated. The BH loops under compressive stress are also roughly reconstructed regardless of the choice of identification method for scalar or vector play model.

APPENDICES

A. ADSM

A.1 ADSM

Fig. 5(a) illustrates a mesoscopic cell called simplified domain structure model (SDSM) [12], which has six domains corresponding to the three easy axes of cubic anisotropy. The ADSM [7] is constructed by assembling the SDSMs (Fig. 5(b)). The magnetization state in each cell (SDSM) is represented by the volume ratios r_i and the magnetization vectors $\boldsymbol{m}_i = (\sin\theta_i\cos\phi_i, \sin\theta_i\sin\phi_i, \cos\theta_i)$ ($i = 1 \ldots 6$) of the six domains. These states are determined so as to locally minimize the total magnetic energy e, which consists of the Zeeman energy, crystalline anisotropy energy, magnetostatic energy, and magnetoelastic energy. The magnetomechanical interaction is caused by the magnetoelastic energy.

Local minimization of e is achieved by solving the ordinary differential equations given as

$$\mathrm{d}\boldsymbol{X}/\mathrm{d}t = \boldsymbol{Y},\ \mathrm{d}\boldsymbol{Y}/\mathrm{d}t = -\partial e/\partial \boldsymbol{X} - \beta \boldsymbol{Y} \tag{15}$$

where $\boldsymbol{X} = (\boldsymbol{X}_1, \boldsymbol{X}_2, \ldots)$ represents the state variable vector, $\boldsymbol{X}_j$ consists of $(\theta_{j,1}, \ldots, \theta_{j,6}, \phi_{j,1}, \ldots, \phi_{j,6}, r_{j,1}, \ldots, r_{j,5})$ in cell j, $\boldsymbol{Y}$ is an intermediate variable vector, and β is the dissipation factor. A local energy minimum is obtained by integrating (15) numerically until an equilibrium point at which $\mathrm{d}\boldsymbol{X}/\mathrm{d}t = \mathrm{d}\boldsymbol{Y}/\mathrm{d}t = 0$ is reached.

The magnetostatic energy is the most time-consuming of the components of e to compute. The demagnetizing field $\boldsymbol{H}_{\mathrm{st}}$ in cell j due to the magnetostatic energy is given as

$$\boldsymbol{H}_{\mathrm{st}}(j) = -M_{\mathrm{S}} \sum_{j'} \boldsymbol{N}(j-j')\boldsymbol{m}(j'), \tag{16}$$

where $\boldsymbol{m}(j')$ is the average magnetization in cell j', $\boldsymbol{N}$ is the demagnetizing coefficient matrix, M_{S} is the magnitude of the spontaneous magnetization, and j and j' are cell indices. To avoid the convolution in (16) due to the dipole-dipole interaction, the demagnetizing field is assumed to be determined predominantly by thin-sheet geometry, which derives an independent-particle approximation [9] as:

$$\boldsymbol{H}_{\mathrm{st}}(j) = -M_{\mathrm{S}}\boldsymbol{N}'\boldsymbol{m}(j). \tag{17}$$

Therein $\boldsymbol{N}' = \sum_{j''} \boldsymbol{N}(j'')$ is the macroscopic demagnetizing coefficient matrix. This paper uses (17) for simplicity in the magnetostatic computation.

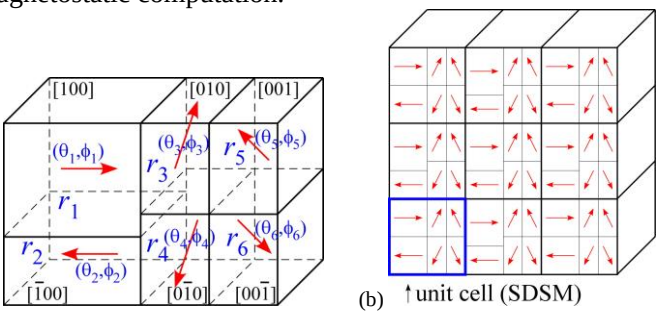

Fig. 5. Schematics of ADSM: (a) mesoscopic six-domain particle (SDSM) and (b) ADSM consisting of assembly of mesoscopic particles.

A.2 Pinning field

The macroscopic relationship between the normalized magnetization m and the applied field h in a cell is assumed to be represented as

$$h = h_{\mathrm{ah}}(m) + h_{\mathrm{pn}}(m), \tag{18}$$

where $h_{\mathrm{ah}}(m)$ represents the anhysteretic magnetization property and $h_{\mathrm{pn}}(m)$ is the pinning field. The anhysteretic field is determined by the Zeeman energy, crystalline anisotropic energy, magnetostatic energy, and magnetoelastic energy. In the previous studies, the hysteretic property of h_{pn} is represented by the scalar stop model as mentioned in Subsection 2.1. In the ADSM, h_{pn} appears as a component of $\partial e/\partial \boldsymbol{X}_j$ with respect of $r_{j,i}$ as

$$\partial e_{\mathrm{pn}} / \partial r_{j,i} = 2h_{\mathrm{pn}}(2r_{j,i} - 1). \tag{19}$$

where e_{pn} is the pinning energy. Note that e_{pn} itself is not necessary to give the pinning field.

B. Comparison with Stop Model

The unweighted pinning field model of (1) based on the stop model does not always give accurate results without some adjustments. Therefore, the stop-based model with the weighted pinning model similar to that given in (3) is compared with the play-based model, where the scalar play model P is replaced by the scalar stop model S. In a manner similar to the play model version, the scalar stop models S_1, S_2 and S_3 are identified from BH loops that are measured unidirectionally under stress-free conditions [9]. The BH loops that were calculated using S_1, S_2 and S_3 are plotted in Fig. 6. The loops that were yielded by the play model shown in Fig. 3 are smoother than those shown in Fig. 6. Figure 7 shows the stress dependence of the hysteresis loss per cycle given by the stop model, which is as accurate as the play model for compressive stress but is not very accurate for tensile stress.

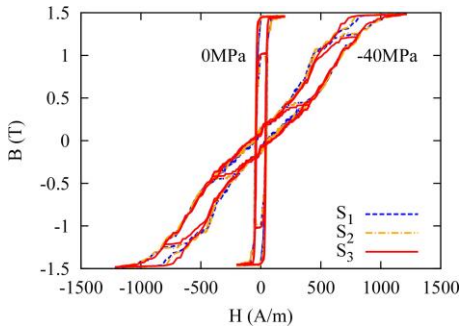

Fig. 6. BH loops simulated using scalar stop models for pinning field representation.

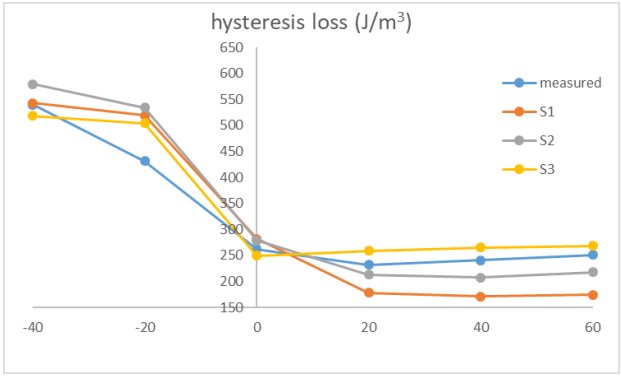

Fig. 7. Stress dependence of hysteresis loss simulated using stop models S_1, S_2 and S_3 for pinning field representation.

Acknowledgments

Funding: This work was supported in part by the Japan Society for the Promotion of Science under a Grant-in-Aid for Scientific Research (C) [grant number 17K06300]. We thank David MacDonald, MSc, from Edanz Group (www.edanzediting.com/ac) for editing a draft of this manuscript.

References

[1] Y. Kai, Y. Tsuchida, T. Todaka, M. Enokizono, "Influence of stress on vector magnetic property under alternating magnetic flux conditions," *IEEE Trans. Magn.*, vol. 47, pp. 4344- 4347, 2011.

[2] M. LoBue, C. Sasso, V. Basso, F. Fiorillo, G. Bertotti, "Power losses and magnetization process in Fe Si non-oriented steels under tensile and compressive stress," *J. Magn. Magn. Mater.*, vol. 215-216, pp. 124-126, 2000.

[3] N. Leuning, S. Steentjes, K. Hameyer, M. Schulte, W. Bleck, "Effect of material processing and imposed mechanical stress on the magnetic, mechanical, and microstructural properties of high-silicon electrical steel," *Steel Research Intl.*, vol. 87, pp. 1638-1647, 2016.

[4] U. Aydin, P. Rasilo, F. Martin, A. Belahcen, L. Daniel A. Haavisto, A. Arkkio, "Effect of multi-axial stress on iron losses of electrical steel sheets," *J. Magn. Magn. Mater.*, vol. 469, pp. 19–27, 2019.

[5] L. Daniel, M. Rekik, and O. Hubert "A multiscale model for magneto-elastic behaviour including hysteresis effects," *Arch. Appl. Mech.*, vol. 84 pp. 1307-1323, 2014.

[6] B. Sai Ram, A.P.S. Baghela, S.V. Kulkarni, K. Chwastek, L. Daniel, "A hybrid product-multi-scale model for magneto-elastic behavior of soft magnetic materials," *Physica B*, vol. 571, pp. 301–306, 2019.

[7] S. Ito, T. Mifune, T. Matsuo and C. Kaido, "Macroscopic magnetization modeling of silicon steel sheets using the assembly of six-domain particles," *J. Appl. Phys.*, vol. 117, 17D126, 2015.

[8] S. Ito, T. Mifune, T. Matsuo, C. Kaido, Y. Takahashi, and K. Fujiwara, "Simulation of the stress dependence of hysteresis loss using an energy-based domain model," *AIP Advances*, vol. 8, 047501, 2018.

[9] T. Matsuo, Y. Nishimura, Y.Mishima, T. Mifune, Y. Takahashi, K. Fujiwara, "Pinning field modeling using stop hysterons for multi-domain particle model," COMPUMAG Paris, PA-M2, 2019; the full paper version will be appeared in IEEE Xplore Digital Library.
[10] T. Matsuo, D. Shimode, Y. Terada, M. Shimasaki, "Application of stop and play models to the representation of magnetic characteristics of silicon steel sheet, *IEEE Trans. Magn.*, vol. 39, 1361-1364, 2003.
[11] T. Matsuo and M. Shimasaki, "Two types of isotropic vector play models and their rotational hysteresis losses, *IEEE Trans. Magn.*, vol. 44, pp. 898-901, 2008.
[12] T. Matsuo, "Magnetization process analysis using a simplified domain structure model," *J. Appl. Phys.*, vol. 109, 07D332, 2011.
[13] T. Matsuo and M. Shimasaki, "Identification of a generalized 3-D vector hysteresis model through the superposition of stop- and play-based scalar models, *IEEE Trans. Magn.*, vol. 43, pp. 2965-2967, 2007.
[14] Kurita, N., Takahashi, Y., Fujiwara, K., Ishihara Y., "Magnetic field analysis taking account of stress-dependent magnetic properties of non-oriented electrical steel sheets," Proc. 18th COMPUMAG, Sydney, Australia, PD7.7, 2011.
[15] F. Fiorillo, *Characterization and Measurement of Magnetic Materials*, Academic Press, 2005.
[16] F. Fiorillo, G. Bertotti, C. Appino, M. Pasquale, "Soft magnetic materials," in *the Wiley Encyclopedia of Electrical and Electronics Engineering*, Wiley online library, 2016.
[17] F. Fiorillo, "Magnetic materials for electrical applications: a review," INRIM Technical Report. 13/2010, March 2010.